

University of Groningen

Development of a Coil Driver for Magnetic Manipulation Systems

Kaya, Mert; Sakthivel, Uthvag; Khalil, Islam S. M.; Misra, Sarthak

Published in:
IEEE magnetics letters

DOI:
[10.1109/LMAG.2019.2935050](https://doi.org/10.1109/LMAG.2019.2935050)

IMPORTANT NOTE: You are advised to consult the publisher's version (publisher's PDF) if you wish to cite from it. Please check the document version below.

Document Version
Publisher's PDF, also known as Version of record

Publication date:
2019

[Link to publication in University of Groningen/UMCG research database](#)

Citation for published version (APA):

Kaya, M., Sakthivel, U., Khalil, I. S. M., & Misra, S. (2019). Development of a Coil Driver for Magnetic Manipulation Systems. *IEEE magnetics letters*, 10, [2104905]. <https://doi.org/10.1109/LMAG.2019.2935050>

Copyright

Other than for strictly personal use, it is not permitted to download or to forward/distribute the text or part of it without the consent of the author(s) and/or copyright holder(s), unless the work is under an open content license (like Creative Commons).

The publication may also be distributed here under the terms of Article 25fa of the Dutch Copyright Act, indicated by the "Taverne" license. More information can be found on the University of Groningen website: <https://www.rug.nl/library/open-access/self-archiving-pure/taverne-amendment>.




Take-down policy

If you believe that this document breaches copyright please contact us providing details, and we will remove access to the work immediately and investigate your claim.

Downloaded from the University of Groningen/UMCG research database (Pure): <http://www.rug.nl/research/portal>. For technical reasons the number of authors shown on this cover page is limited to 10 maximum.

Electromagnetics

Development of a Coil Driver for Magnetic Manipulation Systems

Mert Kaya^{1,2} , Uthvag Sakthivel¹, Islam S. M. Khalil¹ , and Sarthak Misra^{1,2} ¹*Surgical Robotics Laboratory, Department of Biomechanical Engineering, University of Twente, 7522 NB Enschede, The Netherlands*²*Department of Biomedical Engineering and University Medical Centre Groningen, University of Groningen, 9713 AV Groningen, The Netherlands*

Received 28 May 2019, revised 25 Jun 2019, accepted 19 Jul 2019, published 13 Aug 2019, current version 20 Sep 2019.

Abstract—Pulsewidth modulation (PWM) is the most commonly used technique to drive electromagnetic coils in magnetic manipulation systems. Relatively low PWM frequencies generate high-magnitude current ripple and magnetic field fluctuation. In this letter, coils are powered by a driver at PWM frequencies close to their self-resonant frequencies to generate high-frequency magnetic fields and minimize current ripple and magnetic field fluctuation. In order to protect the driver against the penetration of stray electromagnetic and magnetic fields, a multilayer shielding enclosure is employed. The coil driver is used to study the effect of varying PWM frequencies on current, magnetic field, and ohmic loss using Helmholtz, air, and iron core coils. The current ripple magnitude is significantly minimized when the coils are driven at PWM frequencies close to their self-resonant frequencies. This results in reduction of magnetic field fluctuation and provides more accurate measurement of magnetic field magnitude. Our experiments show that increasing the PWM frequency from 100 Hz to 25 kHz decreases the current ripple and magnetic fluctuation by two orders of magnitude, with a negligible effect on the ohmic loss.

Index Terms—Electromagnetics, coil drive, current ripple minimization, magnetic field fluctuation, ohmic loss, pulsewidth modulation.

I. INTRODUCTION

The field of magnetic manipulation has been witnessing substantial progress in recent years. Its most prominent application domains are minimally invasive surgery, drug delivery, and assembly of microscale objects [Nelson 2010, Diller 2014, Heunis 2018]. Electromagnetic coils produce magnetic fields by inducing current through the loops. These coils are used in magnetic manipulation systems by adjusting the amplitude of the current [Kummer 2010]. Pulsewidth modulation (PWM) is the most frequently used technique to control the current, since it provides high efficiency, low power loss, and robustness to noise [Ma 2003]. However, PWM produces high-magnitude current ripples at relatively low frequencies. As a result of the current ripples, magnetic field fluctuation occurs. These fluctuations limit the operating time of the coils and decrease the predictability of the field, which is an essential component for the manipulation.

Although coil configuration has been extensively studied for magnetic manipulation systems, there is a lack in the literature regarding development of coil drivers for precise magnetic manipulation [Kratovichil 2009, Diller 2013, Boskma 2016, Charreyron 2017, Abbott 2018]. The relationship between PWM frequency and magnetic field fluctuation has not been considered. The majority of drivers used in the literature are designed for low-frequency drive applications. PWM resolution in such drivers also changes with the PWM frequency, which leads to relatively low motion resolution for the manipulation.

In this letter, a coil driver is developed to minimize the magnetic field fluctuations and improve the motion resolution of magnetic ma-

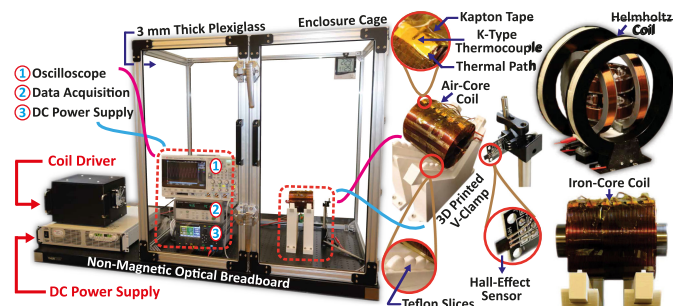


Fig. 1. Overview of the experimental setup used for monitoring effect of varying PWM frequencies on the current through coil terminals, magnetic field, and ohmic loss using the coil driver.

nipulation systems. A multilayer shielding enclosure is specifically machined to protect the driver by blocking stray magnetic and electromagnetic fields. Unlike the drivers used in magnetic manipulation systems, coils are driven at higher PWM frequencies, which are close to their self-resonant frequencies using the developed coil driver [Mao 1996, Patella 2003, Oliveira 2007, Shirabe 2012, Han 2017]. This method minimizes magnetic field fluctuation by reducing current ripple magnitude, which provides a more predictable field. In addition, the developed driver is essential for the applications where high-frequency magnetic field generation is required, such as hyperthermia-based drug delivery using magnetic microagents [Kumar 2011]. Magnetic manipulation and drug release can be performed using the developed driver without an external magnetic induction unit, which decreases the complexity of the system. The driver is experimentally validated using Helmholtz, air, and iron core coils. At varying PWM frequencies, current through coil terminals, magnetic field magnitude, and ohmic loss is monitored (see Fig. 1). Finite element analysis is also performed to

Corresponding author: Mert Kaya (e-mail: m.kaya@utwente.nl).

This letter has supplementary downloadable material available at <http://ieeexplore.ieee.org>, provided by the authors. The material consists of a video demonstrating the simulation results.

Digital Object Identifier 10.1109/LMAG.2019.2935050

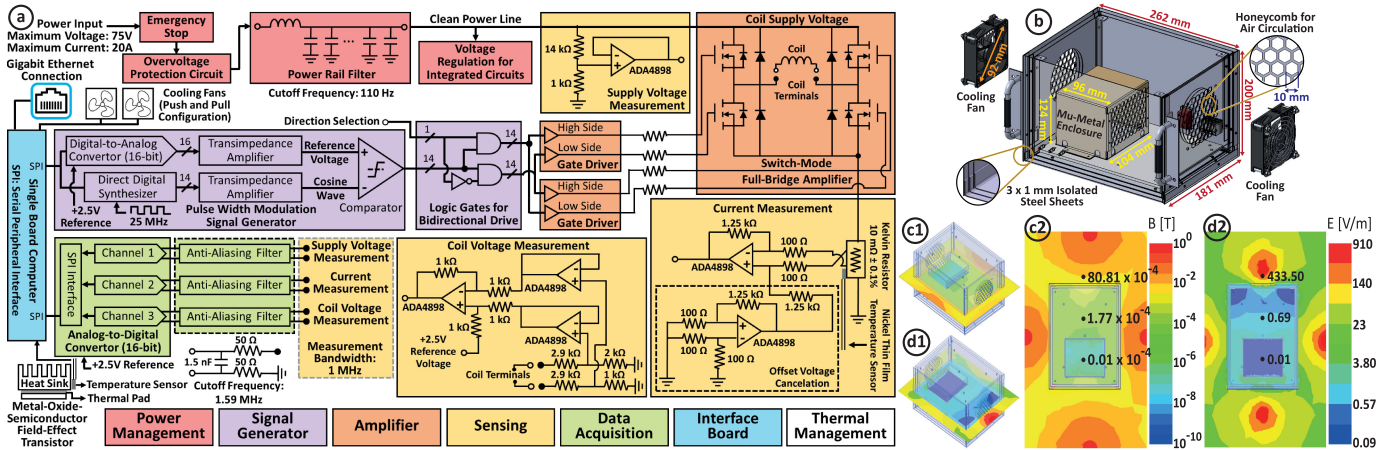


Fig. 2. Schematic representation of the coil driver. (a) Architecture of the driver circuit. (b) Computer-aided design model of the machined multilayer shielding enclosure. (c) and (d) Finite element results for the attenuation efficiency of the electromagnetic and magnetic shielding enclosure. Magnetic and electromagnetic field distributions in and around the shielding enclosure are shown in (c), (d) and (e), (f), respectively.

simulate the effect of varying PWM frequencies on the current, magnetic field, ohmic loss, and magnetic force. In the following section, coil driver architecture is explained. The experimental setup and our results are presented in Section III.

II. COIL DRIVER

A. Driver Architecture

The lumped element model of a coil consists of an inductor (L) in series with a resistor (R) and a capacitor (C) connected in parallel with L and R [Oliveira 2007]. When the voltage is applied to the coil, current reaches its steady-state value at five times coil time constant (5τ). τ is the required time for a current to reach its 63.2% steady-state value and calculated as L/R . If the PWM signal with a frequency of $1/(5\tau)$ is applied to coils, a sawtooth current waveform (also known as current ripple) is observed. The peak-to-peak amplitude of the current ripple minimizes when PWM frequency is on the order of $1/(5\tau)$. The frequency can be increased up to coil self-resonant frequency ($1/(2\pi\sqrt{LC})$), since exceeding self-resonant frequency results in capacitive behavior of the coil. This can also be observed from frequency (f) dependent impedance analysis of the coil ($(R + j2\pi fL)/(j2\pi fCR - (2\pi f)^2LC + 1)$). In order to drive the coils at PWM frequencies that are close to their self-resonant frequencies, a coil driver is developed.

The developed coil driver architecture is illustrated in Fig. 2(a). The driver circuit is capable of generating a 14-bit PWM signal and amplifying it up to 1 MHz. A PWM signal with 14-bit resolution is generated by a comparator using a cosine wave with reference voltage. PWM carrier frequency and duty cycle are adjusted by changing the frequency of the cosine wave and level of reference voltage, respectively. Cosine waves at desired frequency and reference voltage are generated using a 14-bit direct digital synthesizer (DDS) and a 16-bit digital-to-analog converter (DAC), respectively. Outputs of both DDS and DAC are currents that provide high slew rate and robustness to noise. A transimpedance amplifier is used to convert the output of DDS and DAC currents to voltage. In order to use a single-channel PWM signal for the bidirectional coil drive, a combination of logic gates is configured. The generated PWM signal has a constant res-

olution of up to 1 MHz, unlike conventional drivers. It is amplified using a switch-mode full-bridge amplifier consisting of four metal-oxide-semiconductor field-effect transistors (MOSFETs) driven by two gate drivers. In order to get a precise coil drive, fluctuation in the power line during the switching is filtered using a specifically designed passive power rail filter with a cutoff frequency of 110 Hz.

Accurate sensing of current through coil terminals is one of the vital elements of any designed driver for a precise magnetic manipulation, since current data are fed back to the controllers. For current sensing, a four-wire Kelvin resistor is connected between the full-bridge amplifier and ground. The output of the Kelvin resistor is connected to a differential amplifier. An offset measurement circuit is built to cancel the inherent offset voltage of the differential amplifier. To measure offset voltage of the amplifier, a second differential amplifier circuit is built, and its outputs are connected to the ground [Roberge 1975]. Since the voltage difference between input terminals is zero, the output signal equals offset voltage of the amplifier. The signal that is obtained using this circuit is subtracted from the differential input signal for relatively accurate measurements. In addition, a temperature sensor is placed on the Kelvin resistor to compensate resistor change related to temperature. Noise characterization of the driver is done by supply and coil voltage measurement circuits. A 16-bit analog-to-digital converter (ADC) is used to digitize outputs of current and voltage measurement circuits. Antialiasing filters are placed between the measurement circuit outputs and ADC to filter high-frequency noise. Utilizing the current and voltage measurement circuits, the impedance curve of the coils is obtained. A single-board computer (SBC) establishes communication with both the ADC and PWM generator via serial peripheral interface. The driver is cooled by two SBC-controlled fans placed as push and pull configurations [Farnsworth 2006]. MOSFET cooling is additionally maintained by attached heat sinks. Temperature sensors placed on the heat sink surfaces provide feedback to adjust fan speed.

B. Magnetic and Electromagnetic Shielding

Magnetic manipulation systems inherently generate stray magnetic and electromagnetic fields that might damage the driver electronics, since they significantly degrade the accuracy of measurement and control signals. To prevent possible interference, a shielding enclosure is

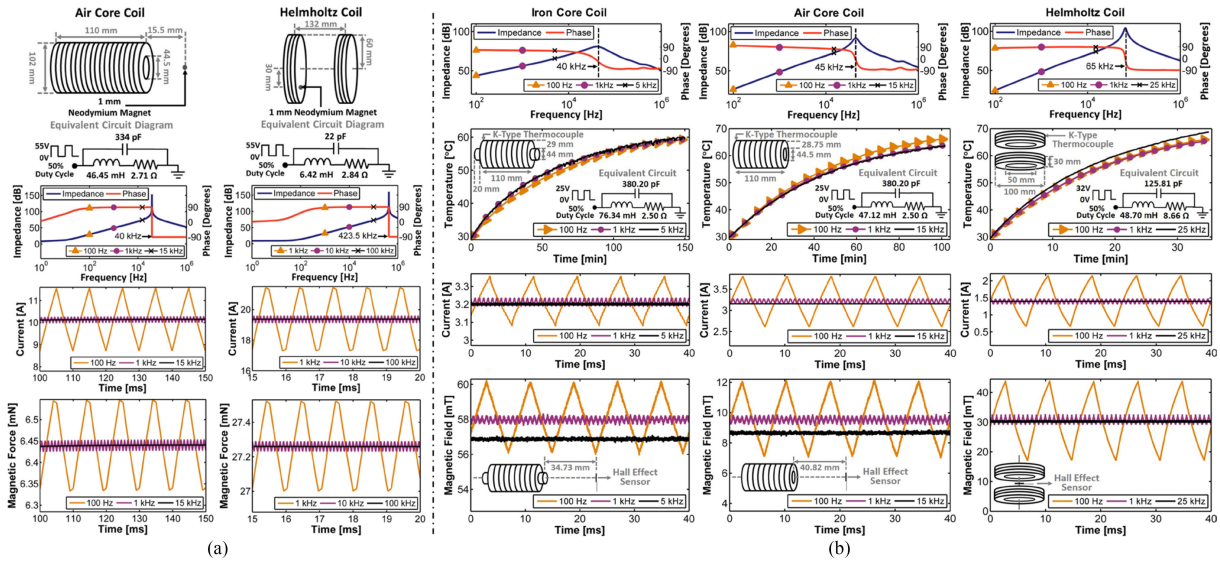


Fig. 3. Finite element and experimental results. (a) Finite element results of magnetic force acting on a magnet are shown for air core and Helmholtz coils. (b) Experimental results of coil drive are shown for iron core, air core, and Helmholtz coils.

machined using both 1 mm thickness steel (CR4, cold rolled) and Mu-metal. Although steel has high relative permeability of 100 to 5000 and generates a low-resistance path for both electromagnetic and magnetic fields, it might not be enough to attenuate the magnitude of stray fields [Cho 2018]. On the other hand, Mu-metal that is a Ni-Fe alloy provides extremely high relative permeability of 80 000 to 100 000 and stronger shielding [Whelan 2018]. When steel and Mu-metal are used together, interference is attenuated by steel as a preprocessing step layer then removed by Mu-metal. Path resistance is decreased by increasing the number of steel sheets, known as multilayer shielding [Yashchuk 2013, Bachir 2016]. Therefore, three individual steel sheets are placed in parallel and isolated using two three-dimensional (3-D) printed dividers. Inside of these steel layers, a Mu-metal enclosure is placed to protect sensitive driver parts. Honeycomb structures are placed onto the side surfaces of the steel and the Mu-metal enclosures to circulate air with fans. A schematic of the shielding enclosure is illustrated in Fig. 2(b).

III. EXPERIMENTS

A. Finite Element Results

Finite element analysis using ANSYS Electronics (Swanson Analysis Systems, Inc., Canonsburg, PA, USA) was performed to simulate magnetic field fluctuation, ohmic loss, and magnetic force. Air, vacoflux, and iron core coils were used to visualize both fluctuation and ohmic loss at varying PWM frequencies. Furthermore, magnetic field fluctuation in and around the Helmholtz coil was simulated to monitor coupling between the coil pair. Dimensions, equivalent circuits, and computed impedance and phase curves of both air core and Helmholtz coils are given in Fig. 3(a). PWM at varying frequencies with 55 V amplitude and 50% duty cycle was applied to the coils for extreme boundary conditions.

Simulations were run with 15, 5, and 1 kHz PWM frequencies for air, vacoflux, and iron core coils, respectively. Low-frequency response of the coils was simulated at 100 Hz. The Helmholtz coil was simulated at 1, 10, and 100 kHz. Simulations show that substantial magnetic field fluctuation occurs at low frequencies,

whereas fluctuation is significantly reduced at high frequencies [see Fig. 3(a)]. Substantially improved coupling between Helmholtz pair and a more uniform magnetic field were observed compared to the low PWM frequency. Furthermore, the increase in PWM frequency does not highly affect ohmic loss. Please refer to the supplementary video that demonstrates the simulation results.

The effect of PWM frequency on magnetic force ripple acting on a 1 mm spherical magnet using air core and Helmholtz coils was simulated. The magnet locations are depicted in Fig. 3(a). In order to monitor the relationship between PWM frequency and magnetic force, the air core coil was simulated at 100 Hz, 1 kHz, and 15 kHz. Force ripple magnitudes at these frequencies were computed as 0.22, 0.14, and 0.01 mN, respectively. For Helmholtz coil, force magnitude ripples at 1, 10, and 100 kHz were computed as 0.52, 0.19, and 0.02 mN, respectively. In both of these simulations, the force ripple magnitude was reduced by nearly 96% when the PWM frequency was changed from lowest to highest frequency. Current and magnetic force waveforms are plotted in Fig. 3(a).

Electromagnetic and magnetic field attenuation efficiency of the shielding enclosure was computed using four air core coils and four dipole antennas. Coils and antennas were arranged to generate 8 mT magnetic field and 430 V/m electric field on the side surfaces of the enclosure, respectively. Magnetic and electromagnetic field distributions are shown in Fig. 2(c) and (d). The multilayer steel configuration attenuates magnetic and electromagnetic signal amplitudes by 97.82% and 99.99%, respectively [see Fig. 2(c) and (d)]. Furthermore, attenuated wave magnitudes by the steel is degraded by 99.99% inside Mu-metal. Results show that combination of steel and Mu-metal provides strong blockage against electromagnetic and magnetic contamination.

B. Experimental Setup

Helmholtz, air and iron core coils were used to test performance of the coil driver at varying PWM frequencies. A Hall-effect sensor (49E, YZPST, China) was used to monitor high-frequency fluctuation in the magnetic field. The sensor was supplied with a dc power supply (E36313A, Keysight, Santa Rosa, CA, USA), and its analog

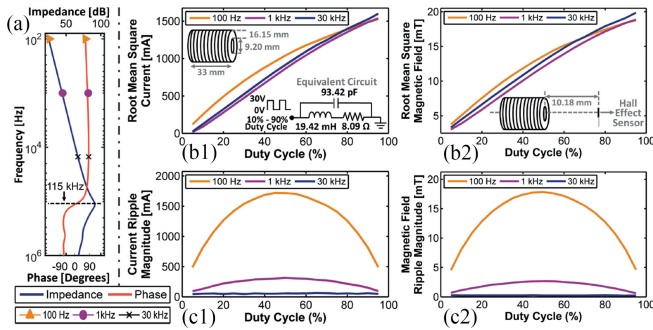


Fig. 4. Experimental results of coil drive with varying duty cycles. (a) Impedance and phase curves of the air core coil used. RMS current and magnetic field magnitudes versus duty cycle are shown in (b1) and (b2), respectively. Current and magnetic field ripple magnitudes versus duty cycle are shown in (c1) and (c2), respectively.

output was acquired using an oscilloscope (DSOX3014T, Keysight). In order to provide a disturbance-free measurement environment, the experimental setup was mounted on a nonmagnetic optical breadboard (PBG52514, ThorLabs, Newton, NY, USA). Coil surface temperature was measured to observe ohmic losses using six K-type thermocouples (34307A, Keysight). Temperature data were acquired using a data acquisition unit (34901A and 34972A, Keysight) with a sampling rate of 1 Hz. In order to provide the same air convection conditions during the experiments, an enclosure cage with a volume of $670 \times 920 \times 950 \text{ mm}^3$ was fabricated [Inan 2014, Uras 2017]. The cage was specifically sealed to avoid any external air flow and keep the effect of coil temperature on the global temperature at minimum to accurately measure ohmic loss and eliminate disturbance inside the enclosure cage. Air and iron core coils were placed onto a custom-made 3-D printed V-clamp. Teflon slices were placed between the clamp and the coil to prevent temperature rise and heat conduction. The driver was supplied with a dc power supply (N8738A, Keysight). The experimental setup is shown in Fig. 1.

C. Experimental Results

Impedance and phase curves were analyzed using a Hewlett Packard 4194 A impedance/gain-phase analyzer to determine equivalent circuits and self-resonance frequencies of the coils. Frequency-dependent impedance and phase plots, the equivalent circuits, and dimensions of the coils are plotted in the first two rows of Fig. 3(b). The self-resonance frequencies of iron core, air core, and Helmholtz coils were measured as 40, 45, and 65 kHz, respectively. During the experiments, coil surface temperature, current through coil terminals, and fluctuation in magnetic field at a specified location were monitored at varying PWM frequencies with 50% duty cycle. Experiments were carried out to monitor low- and high-frequency behavior of each coil configuration under constant PWM duty cycle and supply voltage. All of the coil configurations were driven at 100 Hz and 1 kHz to observe their low-frequency behavior. In order to monitor high-frequency behavior of the coils, iron core, air core, and Helmholtz coils were driven at 5, 15, and 25 kHz, respectively. These frequencies were chosen to keep the magnitude of current ripple below 20 mA. PWM signal amplitude was set to 32 and 25 V for Helmholtz, air core, and iron core coils, respectively. The effect of duty cycle on current and magnetic field

Table 1. Mean, standard deviation (std), ripple magnitude (ripple), and rms of current and magnetic waveforms are presented to show the effect of PWM frequency on current and magnetic field.

	PWM Frequency	Current (mA)				Magnetic Field (mT)			
		Mean	Std	Ripple	RMS	Mean	Std	Ripple	RMS
Iron Core Coil	100 Hz	3,218	75.4	280.2	3,219	58.1	1.2	4.3	58.1
	1 kHz	3,212	14.8	51.5	3,212	58.0	0.1	0.7	58.0
	5 kHz	3,199	4.6	18.9	3,199	56.9	0.1	0.5	56.9
Air Core Coil	100 Hz	3,210	347.2	1,197.2	3,228	9.6	1.4	5.2	9.7
	1 kHz	3,217	35.4	120.6	3,217	9.5	0.2	0.8	9.5
	15 kHz	3,156	1.9	10.1	3,156	8.7	0.1	0.5	8.7
Helmholtz Coil	100 Hz	1,409	447.3	1,497.0	1,478	30.4	7.9	27.1	31.4
	1 kHz	1,397	47.0	167.3	1,397	30.6	0.8	3.7	30.6
	25 kHz	1,397	1.6	9.0	1,397	30.0	0.3	1.1	30.0

ripples was observed by driving an air core coil with 115 kHz self-resonant frequency. Impedance and phase plots, the equivalent circuit, and dimensions of the coil are shown in Fig. 4(a) and (b). The coil was driven with varying duty cycles starting from 5% to 95% with 5% increment at 100 Hz, 1 kHz, and 30 kHz. PWM signal amplitude was set to 30 V to pass 1500 mA root-mean-square (RMS) current from the coil when the duty cycle was 90%.

In order to monitor ohmic losses, coil surface temperature was recorded until it exceeded 60°C , since saturation temperatures of the coil configurations were between 60 and 80°C . Initial coil surface temperatures were kept as 29°C . Temperature plots are shown in the second row of Fig. 3(b). Ohmic loss change between low and high frequencies is negligible, as observed in the finite element analysis.

Current and magnetic field waveforms of coils at varying PWM frequencies are plotted in the third and fourth rows of Fig. 3(b), respectively. Mean, standard deviation, and ripple magnitude of current and magnetic waveforms are shown in Table 1. RMS and ripple magnitudes of current and magnetic waveforms at varying duty cycles are plotted in Fig. 4(b) and (c). In accordance with our expectations, magnitudes of current and magnetic ripples are significantly reduced when the coils are driven at PWM frequencies close to their resonance frequencies. When the PWM drive frequency of the Helmholtz coil is changed from 100 Hz to 25 kHz, ripple magnitudes of current and magnetic field are reduced 95.81% and 99.40%, respectively. Hence, driving coils at high frequencies provide nearly two orders of magnitude reduction in ripple magnitudes. This results in the increasing predictability of the field.

RMS values of both the magnetic field and current magnitudes in response to low and high PWM frequencies are close to each other, although there is a significant difference between the ripple magnitudes (see Fig. 4 and Table 1). Even though teslameters have been used for measuring the rms value of the magnetic field waveforms in magnetic manipulation studies, they are not suitable for monitoring magnetic field fluctuation at both low and high frequencies [Tokarev 2012, Schuerle 2013, Youakim 2015]. This leads to poor current to the magnetic field map, which is one of the key components for magnetic manipulation. On the other hand, the experimental setup presented in this letter provides the instantaneous magnitude of the magnetic field and holds a great promise for accurate measurement of both current and magnetic field ripple magnitudes. Besides, the setup significantly minimizes magnetic field magnitudes by driving the coils at higher PWM frequencies. Thus, overall efficiency is significantly improved for precise magnetic manipulation.

ACKNOWLEDGMENT

The authors thank O. Dalgic, A. Patel, A. Zeybek, A. Akhtayar, and C. M. Heunis for their technical assistance for the construction of experimental setup and P. K. Isgor for her valuable feedback during preparation of this letter. This work was supported by the European Research Council under the European Union's Horizon 2020 Research and Innovation programme under Grant 38428—project ROBOTAR: Robot-Assisted Flexible Needle Steering for Targeted Delivery of Magnetic Agents.

REFERENCES

- Abbott J J, Osting B (2018) "Optimization of coreless electromagnets to maximize field generation for magnetic manipulation systems," *IEEE Magn. Lett.*, vol. 9, 1300104, doi: [10.1109/LMAG.2017.2768021](https://doi.org/10.1109/LMAG.2017.2768021).
- Bachir G, Abdechafik H, Mecheri K (2016) "Comparison electromagnetic shielding effectiveness between single layer and multilayer shields," in *Proc. 51st Int. Univ. Power Eng. Conf.*, pp. 1–5, doi: [10.1109/UPEC.2016.8114106](https://doi.org/10.1109/UPEC.2016.8114106).
- Boskma K J, Scheggi S, Misra S (2016) "Closed-loop control of a magnetically-actuated catheter using two-dimensional ultrasound images," in *Proc. IEEE Int. Conf. Biomed. Robot. Biomechatronics*, pp. 61–66, doi: [10.1109/BIOROB.2016.7523599](https://doi.org/10.1109/BIOROB.2016.7523599).
- Charreyron S L, Zeydan B, Nelson B J (2017) "Shared control of a magnetic microcatheter for vitreoretinal targeted drug delivery," in *Proc. IEEE Int. Conf. Robot. Autom.*, pp. 4843–4848, doi: [10.1109/ICRA.2017.7989563](https://doi.org/10.1109/ICRA.2017.7989563).
- Cho B L, Park I Y, (2018) "Electron microscope electron gun for facilitating position adjustment and electron microscope including same," U.S. Patent 15 576 687.
- Diller E, Sitti M (2014) "Three-dimensional programmable assembly by untethered magnetic robotic micro-grippers," *Adv. Functional Mater.*, vol. 24, pp. 4397–4404, doi: [10.1002/adfm.201400275](https://doi.org/10.1002/adfm.201400275).
- Diller E, Giltinan J, Sitti M (2013) "Independent control of multiple magnetic microrobots in three dimensions," *Int. J. Robot. Res.*, vol. 32, pp. 614–631, doi: [10.1177/0278364913483183](https://doi.org/10.1177/0278364913483183).
- Farnsworth A, Austin P, Lambert J (2006) "Cooling system for a computer environment," U.S. Patent 11 056 300.
- Han D, Morris C T, Lee W, and Sarlioglu B (2017) "Comparison between output CM chokes for SiC drive operating at 20-and 200-kHz switching frequencies," *IEEE Trans. Ind. Appl.*, vol. 53, pp. 2178–2188, doi: [10.1109/TIA.2017.2672919](https://doi.org/10.1109/TIA.2017.2672919).
- Heunis C, Sikorski J, Misra S (2018) "Flexible instruments for endovascular interventions: Improved magnetic steering, actuation, and image-guided surgical instruments," *IEEE Robot. Autom. Mag.*, vol. 25, pp. 71–82, doi: [10.1109/MRA.2017.2787784](https://doi.org/10.1109/MRA.2017.2787784).
- Inan M N, Arik M (2014) "A multi-functional design approach and proposed figure of merits for solid state lighting systems," *J. Solid State Lighting*, vol. 1, doi: [10.1186/2196-1107-1-8](https://doi.org/10.1186/2196-1107-1-8).
- Kratochvil B E, Frutiger D, Vollmers K, Nelson B J, (2009), "Visual servoing and characterization of resonant magnetic actuators for decoupled locomotion of multiple untethered mobile microrobots," in *Proc. IEEE Int. Conf. Robot. Autom.*, pp. 1010–1015, doi: [10.1109/ROBOT.2009.5152633](https://doi.org/10.1109/ROBOT.2009.5152633).
- Kumar C S S R, Mohammad F, (2011) "Magnetic nanomaterials for hyperthermia-based therapy and controlled drug delivery," *Adv. Drug Del. Rev.*, vol. 63, pp. 789–808, doi: [10.1016/j.addr.2011.03.008](https://doi.org/10.1016/j.addr.2011.03.008).
- Kummer M P, Abbott J J, Kratochvil B E, Borer R, Sengul A, Nelson B J (2010) "OctoMag: An electromagnetic system for 5-DOF wireless micromanipulation," *IEEE Trans. Robot.*, vol. 26, pp. 1006–1017, doi: [10.1109/TRO.2010.2073030](https://doi.org/10.1109/TRO.2010.2073030).
- Ma N, Song G (2003), "Control of shape memory alloy actuator using pulse width modulation," *Smart Mater. Struct.*, vol. 12, pp. 712–719, doi: [10.1088/0964-1726/12/5/007](https://doi.org/10.1088/0964-1726/12/5/007).
- Mao H, Boroyevich D, Ravindra A, Lee F C (1996) "Analysis and design of high frequency three-phase boost rectifiers," in *Proc. IEEE Appl. Power Electron. Conf. Expo.*, pp. 538–544, doi: [10.1109/APEC.1996.500494](https://doi.org/10.1109/APEC.1996.500494).
- Nelson B J, Kaliakatsos I K, Abbott J J (2010) "Microrobots for minimally invasive medicine," *Annu. Rev. Biomed. Eng.*, vol. 12, pp. 55–85, doi: [10.1146/annurev-bioeng-010510-103409](https://doi.org/10.1146/annurev-bioeng-010510-103409).
- Oliveira A C, Jacobina C B, Lima A M N (2007) "Improved dead-time compensation for sinusoidal PWM inverters operating at high switching frequencies," *IEEE Trans. Ind. Electron.*, vol. 54, pp. 2295–2304, doi: [10.1109/TIE.2007.894770](https://doi.org/10.1109/TIE.2007.894770).
- Patella B J, Prodic A, Zirger A, Maksimovic D (2003) "High-frequency digital PWM controller IC for DC-DC converters," *IEEE Trans. Power Electron.*, vol. 18, pp. 438–446, doi: [10.1109/TPEL.2002.807121](https://doi.org/10.1109/TPEL.2002.807121).
- Roberge J K, (1975) *Operational Amplifiers: Theory and Practice*, vol. 197. New York, NY, USA: Wiley, ch. 11.
- Schuerle S, Erni S, Flink M, Kratochvil B E, Nelson B J (2013) "Three-dimensional magnetic manipulation of micro- and nanostructures for applications in life sciences," *IEEE Trans. Magn.*, vol. 49, pp. 321–330, doi: [10.1109/TMAG.2012.2224693](https://doi.org/10.1109/TMAG.2012.2224693).
- Shirabe K, Swamy M, Kang J-K, Hisatsune M, Wu Y, Kebort D, Honea J (2012) "Advantages of high frequency PWM in AC motor drive applications," in *Proc. IEEE Energy Convers. Congr. Expo.*, pp. 2977–2984, doi: [10.1109/ECCE.2012.6342519](https://doi.org/10.1109/ECCE.2012.6342519).
- Tokarev A, Aprelev A, Zakharov M N, Korneva G, Gogotsi Y, Kornev K G (2012) "Multifunctional magnetic rotator for micro and nanorheological studies," *Rev. Sci. Instrum.*, vol. 83, 065110, doi: [10.1063/1.4729795](https://doi.org/10.1063/1.4729795).
- Uras U Z, Arik M, Tamdoğan E (2017) "Thermal performance of a light emitting diode light engine for a multipurpose automotive exterior lighting system with competing board technologies," *J. Electron. Packag.*, vol. 139, 020907, doi: [10.1115/1.4036403](https://doi.org/10.1115/1.4036403).
- Whelan B, Kolling S, Oborn B M, Keall P (2018) "Passive magnetic shielding in MRI-Linac systems," *Phys. Med. Biol.*, vol. 63, 075008, doi: [10.1088/1361-6560/aab138](https://doi.org/10.1088/1361-6560/aab138).
- Yashchuk V V, Lee S-K, Paperno E (2013), "Magnetic shielding," in *Optical Magnetometry*, D. Budker, Ed. Cambridge, U.K.: Cambridge Univ. Press, pp. 225–248, doi: [10.1017/CBO9780511846380.013](https://doi.org/10.1017/CBO9780511846380.013).
- Youakim K, Ehab M, Hatem O, Misra S, Khalil I S M (2015), "Paramagnetic microparticles sliding on a surface: Characterization and closed-loop motion control," in *Proc. IEEE Int. Conf. Robot. Autom.*, pp. 4068–4073, doi: [10.1109/ICRA.2015.7139768](https://doi.org/10.1109/ICRA.2015.7139768).